REGGEOMETRY OF DEEPLY VIRTUAL COMPTON SCATTERING AND EXCLUSIVE VECTOR MESON PRODUCTION AT HERA

S. Fazio

Brookhaven National Laboratory, 11973 Upton NY, USA

R. Fiore, A. Lavorini

Dipartimento di Fisica, Università della Calabria
Istituto Nazionale di Fisica Nucleare, Gruppo Collegato di Cosenza
87036 Arcavacata di Rende, Cosenza, Italy

L. Jenkovszky[†], A. Salii[‡]

Bogolyubov Institute for Theoretical Physics
National Academy of Sciences of Ukraine
03680 Kiev, Ukraine

(Received May 24, 2013)

A Reggeometric (Regge+Geometry) model, based on the observed proportionality between the forward slope of the differential cross section and the interaction radius, the latter depending on virtuality Q^2 of the incoming virtual photon and on the mass M^2 of the produced particle, is constructed. The objective of this study is the dependence of the Reggepole amplitude on the virtuality Q^2 and masses of the external particles, which remains an open problem for the theory. The present analysis is based on the HERA data on Deeply Virtual Compton Scattering (DVCS) and exclusive diffractive Vector Meson Production (VMP). We treat each class of reactions separately, anticipating a further study that will include both a soft and a hard component of the unique Pomeron.

DOI:10.5506/APhysPolB.44.1333
PACS numbers: 12.39.St, 13.60.Fz, 13.60.Le, 13.60.–r

[†] jenk@bitp.kiev.ua
[‡] saliy.andriy@gmail.com

1. Introduction

The forward slope of the differential cross sections for elastic and quasi-elastic reactions, *e.g.* Deeply Virtual Compton Scattering (DVCS) or Vector Meson Production (VMP), is known to be related to the masses/virtualities of the interacting particles. This phenomenon is clearly seen in Fig. 1, where the forward slope $B(\widetilde{Q}^2)$ is plotted against the variable $\widetilde{Q}^2 = Q^2 + M_V^2$. Here, Q^2 and M_V^2 are, respectively, the square of the virtuality and of the mass of the produced particle, and the notation is evident from Fig. 2.

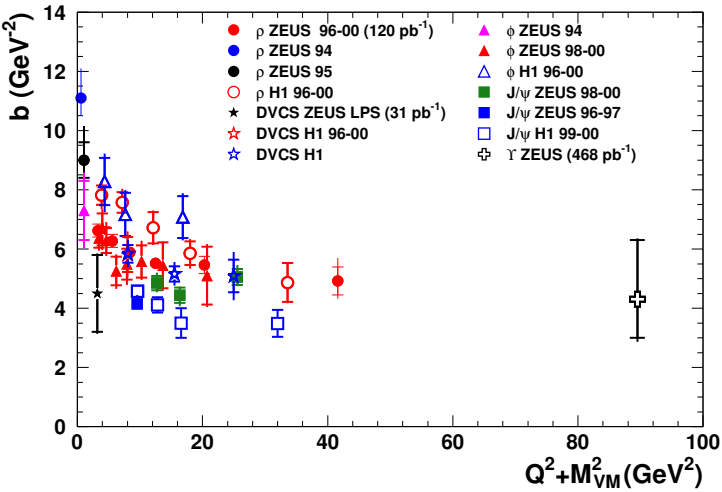

Fig. 1. The forward slope of differential cross sections as a function of $\widetilde{Q}^2 = Q^2 + M_V^2$. Compilation of the data for DVCS and VMP measured by the ZEUS and H1 collaborations, see [1].

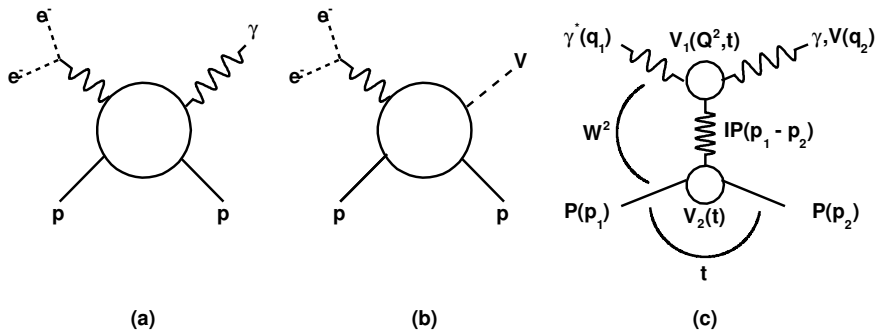

Fig. 2. (a) Diagram of DVCS and (b) diagram of VMP at HERA; (c) DVCS (VMP) amplitudes in a Regge-factorized form.

The slope, proportional to the "interaction radius" $R(\widetilde{Q}^2)$, decreases with increasing $\widetilde{Q}^2$, reaching some saturation value determined by the finite mass of the nucleons in the lower vertex of Fig. 2 (c). Thus, in this "geometrical" picture, the largest slope (radius) is expected for a real Compton scattering, where $\widetilde{Q}^2 = 0$.

In the present paper, we consider exclusive electroproduction of real photons (DVCS) and vector mesons (VMP) making use of the above geometrical considerations, by writing the scattering amplitude in the form

$$A(s,t) \sim e^{\tilde{b}(\widetilde{Q}^2)t}\,, \tag{1}$$

with $\tilde{b}(\widetilde{Q}^2) \sim 1/f(\widetilde{Q}^2)$. This approach was used in Ref. [2] for the simpler case of photoproduction ($Q^2 = 0$).

The off-mass shell continuation of the S-matrix, or, in particular, the introduction of any dependence of the Regge-pole amplitude on the virtuality, Q^2, and masses of external particles remains an open problem for the theory. Empirically, it was approached in various models of which the best known is the introduction of Q^2-dependent parameters in the Regge (*e.g.* the Pomeron) trajectories, namely, the intercept $\alpha_0 \to \alpha_0(Q^2)$ and the slope $\alpha' \to \alpha'(Q^2)$. Since, by definition (*i.e.* by the Regge-factorization), the trajectory should not depend on the properties (masses and virtualities) of the external particles, such Regge poles and trajectories are called "effective" ones. It is the relevant vertex function that bears information about the masses and virtualities of the particles coupled to them. In Ref. [3] a simple model for DVCS and VMP, based on the use of a new variable defined as $z = t - Q^2$, was put forward.

In the view of the limitations of that model as discussed in [4], below we scrutinize an alternative approach [5, 6] by combining the Regge-pole model with geometrical ideas, resulting in Reggeometry = (Regge + geometry). In the nearly forward direction, where the cross sections decrease almost exponentially, $d\sigma/dt \sim e^{Bt}$, the slope B is related to the interaction radius, which is a function of the inverse mass (virtuality) of the particles

$$B = R^2 \sim 1/f\left(\widetilde{Q}^2\right)\,, \tag{2}$$

reflecting the geometrical nature of the slope, proportional to the "interaction radius", or to the inverse squared masses. More precisely, $B = B_1 + B_2 = R_1^2 + R_2^2$, where the two radii correspond to the lower and upper vertices of Fig. 2. This dependence, Eq. (2), will be given explicitly in Sec. 2.

There are, however, several caveats in this simple and appealing interpretation of the slope, namely:

— The relation $\widetilde{Q}^2 = M_V^2 + Q^2$, is model-dependent; an alternative relation, *e.g.* $\widetilde{Q}^2 = M_V^2 + c\,Q^2$, c being a parameter to be determined by fits to experimental data, is equally legitimate. Another degree of freedom enters putting the factor 4 as denominator in the expression of $\widetilde{Q}^2$, *i.e.* writing $\widetilde{Q}^2 = (M_V^2 + cQ^2)/4$, (see Ref. [1]).

— Empirically, the slope can be given by the relation $B \sim (\widetilde{Q}^2)^{-n}$. It includes an exponent n, with $n > 1$, whose value is not necessarily an integer and may even depend on $\widetilde{Q}^2$ (see, for instance, Fig. 10.26 and Eqs. (10.72)–(10.74) of Ref. [1]).

— Relation (2) was established only within certain classes of reactions, notably VMP, $\gamma(\gamma^*)p \to Vp$. It remains an open question if it is also applicable to DVCS, and, moreover, to purely hadronic reactions.

Studies of all these options involve also s and t dependences of the relevant scattering amplitude. We use simple models of s- and t-dependences to concentrate on the less trivial $\tilde{Q}^2$ dependence. Our model is based on two pillars: the "Reggeometric" form of the amplitude, introduced in Introduction, and its two-component nature. The latter implies that the unique Pomeron has two components — a "soft" and "hard" one, and that their relative weight vary with $\widetilde{Q}^2$, thus providing a unify description of both soft and hard collisions. The model was presented at the 2011 EDS Conference in Quy Nhon [5] and at the Diffraction 2012 Conference at the Canarias [6]. Anticipating a global fit (with a universal set of the free parameters), to appear [7], here we make the first important step by fitting the HERA data on several particular processes to a single Reggeometric term.

This one-component effective model is fitted, one-by-one, to the HERA data on DVCS and VMP. The complete, two-component ("soft" and "hard") model is anticipated in Appendix A.

The paper is organized as follows. In Sec. 2, Reggeometry is introduced. In Sec. 3, we consider a simplified version of the model involving a single term only and fitted to DVCS and a number of VMP data. The resulting fits are shown in Sec. 4.

2. The Reggeometric model

According to the arguments presented in the introduction and in [5, 6], the DVCS or VMP amplitudes of the Reggeometric model with a single Pomeron term can be written as

$$A\left(s,t,M,Q^2\right)=\frac{\widetilde{A_0}}{\left(1+\frac{\widetilde{Q^2}}{Q_0^2}\right)^n}\xi(t)\beta\left(t,M,Q^2\right)\left(s/s_0\right)^{\alpha(t)}, \tag{3}$$

where A_0 is a normalization factor, Q_0^2 is a scale for the virtuality, n is a free parameter with $n>1$, $\xi(t)=e^{-i\pi\alpha(t)}$ is the signature factor, s_0 is a scale for the squared energy and $\alpha(t)$ is the Pomeron trajectory. $\beta(t,M,Q^2)$ is the residue factor to be specified as

$$\beta\left(t,M,Q^2\right)=\exp\left[-2\left(\frac{a}{\widetilde{Q}^2}+\frac{b}{2m_N^2}\right)|t|\right], \tag{4}$$

where a and b are free parameters and m_N is the nucleon mass. Thus

$$A\left(s,t,M,Q^2\right)=\frac{\widetilde{A_0}}{\left(1+\frac{\widetilde{Q^2}}{Q_0^2}\right)^{n_s}}\xi(t)(s/s_0)^{\alpha(t)}e^{-2\left(\frac{a}{\widetilde{Q}^2}+\frac{b}{2m_N^2}\right)|t|}. \tag{5}$$

The differential cross section is

$$\frac{d\sigma}{d|t|}=\frac{\pi}{s^2}\left|A\left(s,t,M,Q^2\right)\right|^2. \tag{6}$$

Using Eq. (5), we get

$$\frac{d\sigma}{d|t|}=\frac{|A_0|^2}{\left(1+\frac{\widetilde{Q^2}}{Q_0^2}\right)^{2n}}(s/s_0)^{2(\alpha(t)-1)}e^{-4\left(\frac{a}{\widetilde{Q}^2}+\frac{b}{2m_N^2}\right)|t|}, \tag{7}$$

where $A_0=\frac{\sqrt{\pi}}{s_0}\widetilde{A_0}$.

Assuming a linear Regge trajectory for the Pomeron $\alpha(t)=\alpha_0-\alpha'|t|$, the differential cross section takes the form

$$\frac{d\sigma}{d|t|}=\frac{|A_0|^2}{\left(1+\frac{\widetilde{Q^2}}{Q_0^2}\right)^{2n}}(s/s_0)^{2(\alpha_0-1)}e^{-\left[2\alpha'\ln(s/s_0)+4\left(\frac{a}{\widetilde{Q}^2}+\frac{b}{2m_N^2}\right)\right]|t|}=Ce^{-B|t|}, \tag{8}$$

where the function $C(s,\tilde{Q}^2)$ is independent of t. From this expression, we obtain the forward slope

$$B\left(s,\widetilde{Q}^2\right)=2\alpha'\ln(s/s_0)+4\left(\frac{a}{\widetilde{Q}^2}+\frac{b}{2m_N^2}\right). \tag{9}$$

Then, the elastic cross section is obtained by integrating the differential cross section. The result, in the case of the linear Regge trajectory, is

$$\sigma = \frac{1}{B}\frac{d\sigma}{dt}\bigg|_{t=0}, \tag{10}$$

and due to Eqs. (7) and (9), it reads

$$\sigma = \frac{|A_0|^2}{\left(1+\frac{\widetilde{Q}^2}{Q_0^2}\right)^{2n}} \frac{\left(\frac{s}{s_0}\right)^{2(\alpha_0-1)}}{2\alpha' \ln(s/s_0) + 4\left(\frac{a}{\widetilde{Q}^2}+\frac{b}{2m_N^2}\right)}. \tag{11}$$

3. Fitting strategy and results

As already mentioned in the introduction, in this paper we consider a simple model with a single term for the Pomeron, "soft" or "hard" — depending on the kinematic region and class of reaction[1]. The expressions for the cross sections and the slope are given by Eqs. (9), (7) and (11).

3.1. Strategy

There are eight free parameters in our model, namely: A_0, Q_0^2, n, α_0, α', a, b and s_0. For simplicity, we set $s_0 = 1.0\ \mathrm{GeV}^2$, so seven free parameters remain: the normalization factor A_0; the scale Q_0^2 for the virtuality; the exponent n for Q-dependent factor in the amplitude; the intercept α_0 and the slope α' of the linear Pomeron trajectory; the two coefficients a and b, which set the Q-dependence for the forward slope. These seven free parameters have been found from the fit to the HERA data on the DVCS and the electroproduction of ϕ and J/ψ mesons. Each process was treated separately.

Each class of reaction contains various measurables *i.e.* the data for the forward slope B, for the differential cross section $d\sigma/d|t|$, and for the integrated cross section σ as function of virtuality Q^2 at fixed energy W, or for the integrated cross section σ as function of the energy W at fixed virtuality Q^2. Thus, for each separate reaction, we fitted $d\sigma/d|t|$, σ and B simultaneously.

The units of the fitted parameters are

$$[A_0] = \frac{\sqrt{nb}}{\mathrm{GeV}}, \quad [n] = [\alpha_0] = 1, \quad [\alpha'] = \mathrm{GeV}^{-2}, \quad [a] = [b] = [Q_0^2] = \mathrm{GeV}^2.$$

[1] In Appendix B, we present a possible alternative, empirical model with $\widetilde{Q}^2$-dependent effective trajectories, mimicking the transition between soft and hard dynamics. This model has been presented at the workshop Diffraction 2012 [6].

3.2. DVCS

Here we fit our model to the data on DVCS published in [8–10]. Notice that for DVCS we have $\widetilde{Q}^2 = Q^2$, since $M_\gamma = 0$ GeV. The resulting fit is shown in Figs. 3–7, with the values of the fitted parameters and the relevant χ^2/dof, given in Table I.

TABLE I

Fitted parameters for DVCS.

A_0	Q_0^2	n	α_0
7.98 ± 0.09	1.00 ± 0.34	1.00 ± 0.04	1.20 ± 0.02
α'	a	b	χ^2/dof
0.01 ± 0.03	1.78 ± 0.19	2.14 ± 0.30	0.85

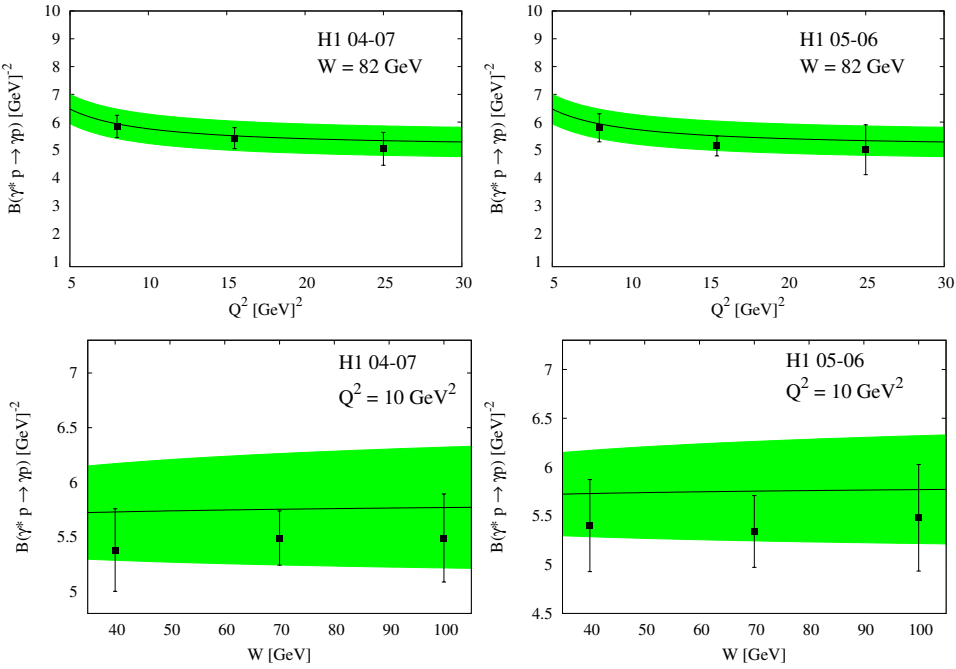

Fig. 3. Fit of Eq. (9) to the H1 data on the forward slopes for $\gamma^* p \to \gamma p$.

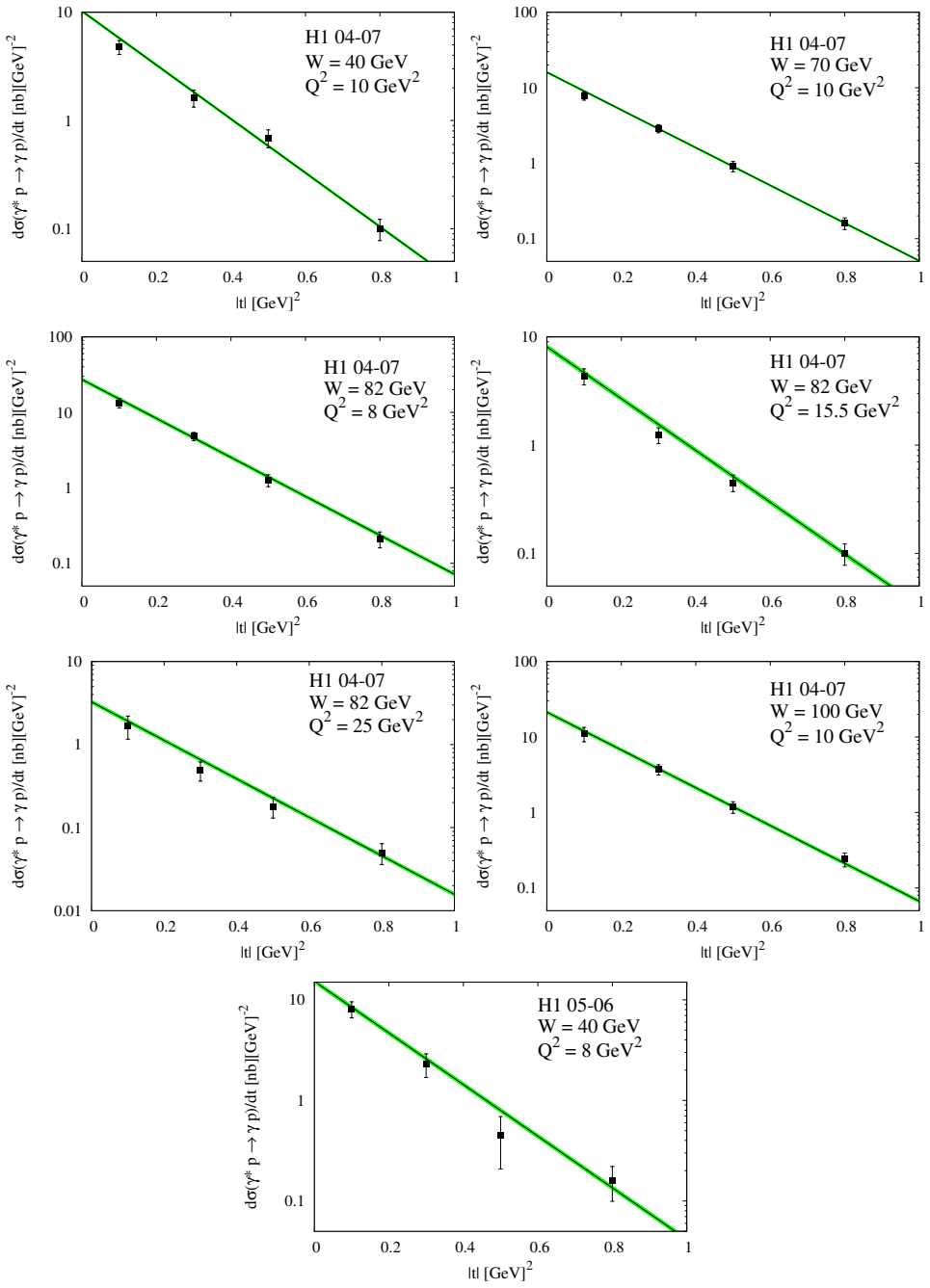

Fig. 4. Fit of Eq. (7) to the H1 data on the differential cross sections for $\gamma^* p \to \gamma p$.

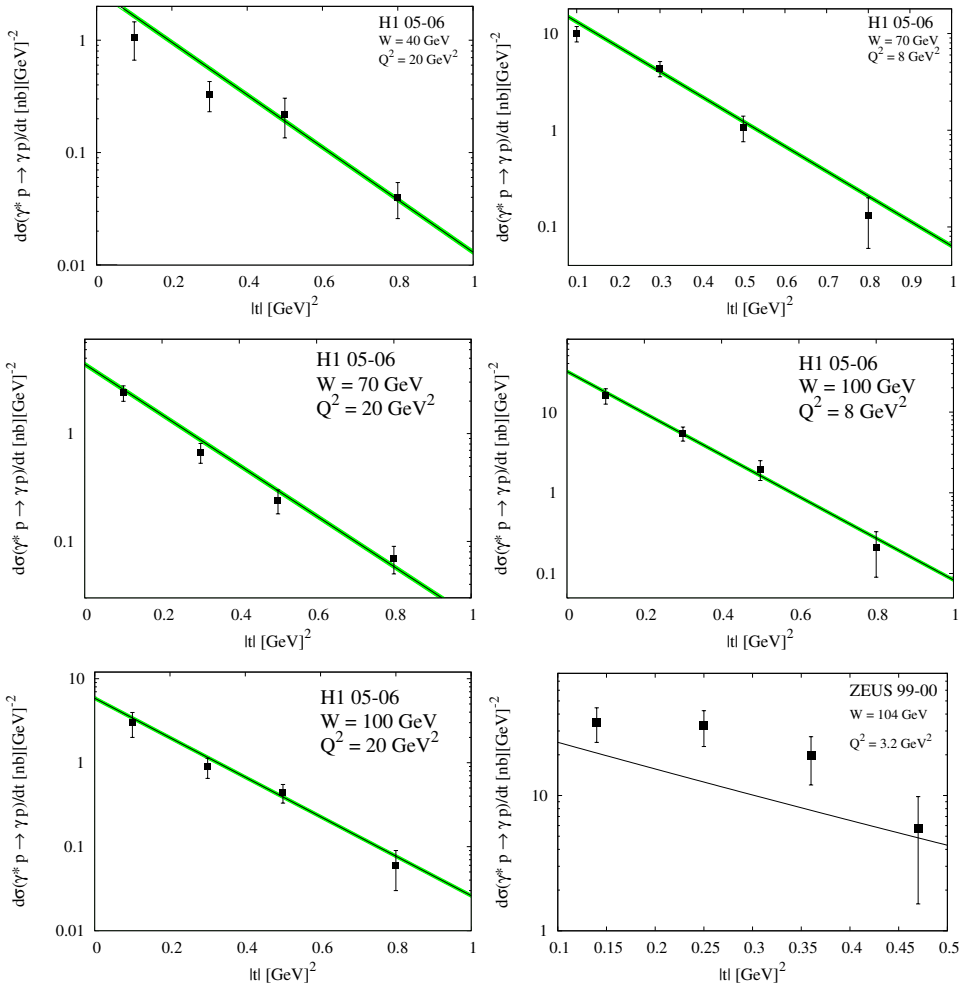

Fig. 5. Fit of Eq. (7) to the H1 an ZEUS data on the differential cross sections for $\gamma^* p \to \gamma p$.

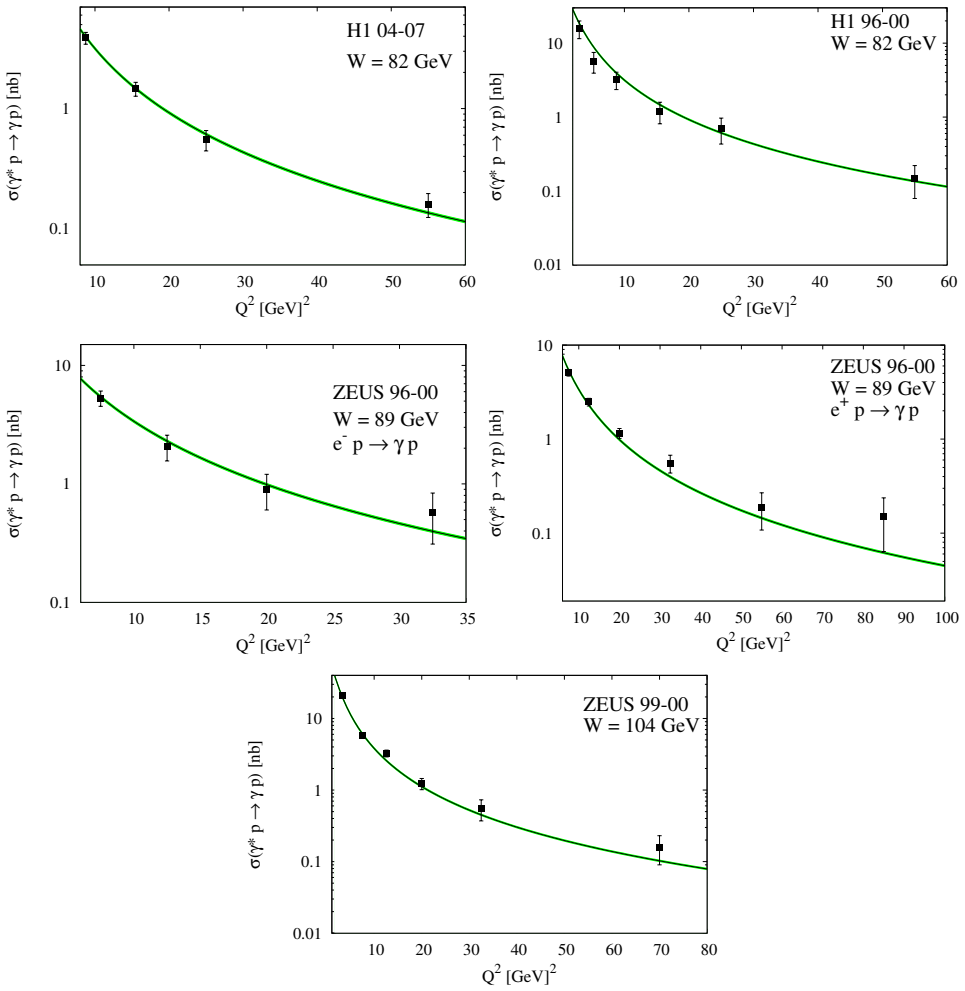

Fig. 6. Fit of Eq. (11) to the H1 and ZEUS data on the integrated cross sections for $\gamma^* p \to \gamma p$.

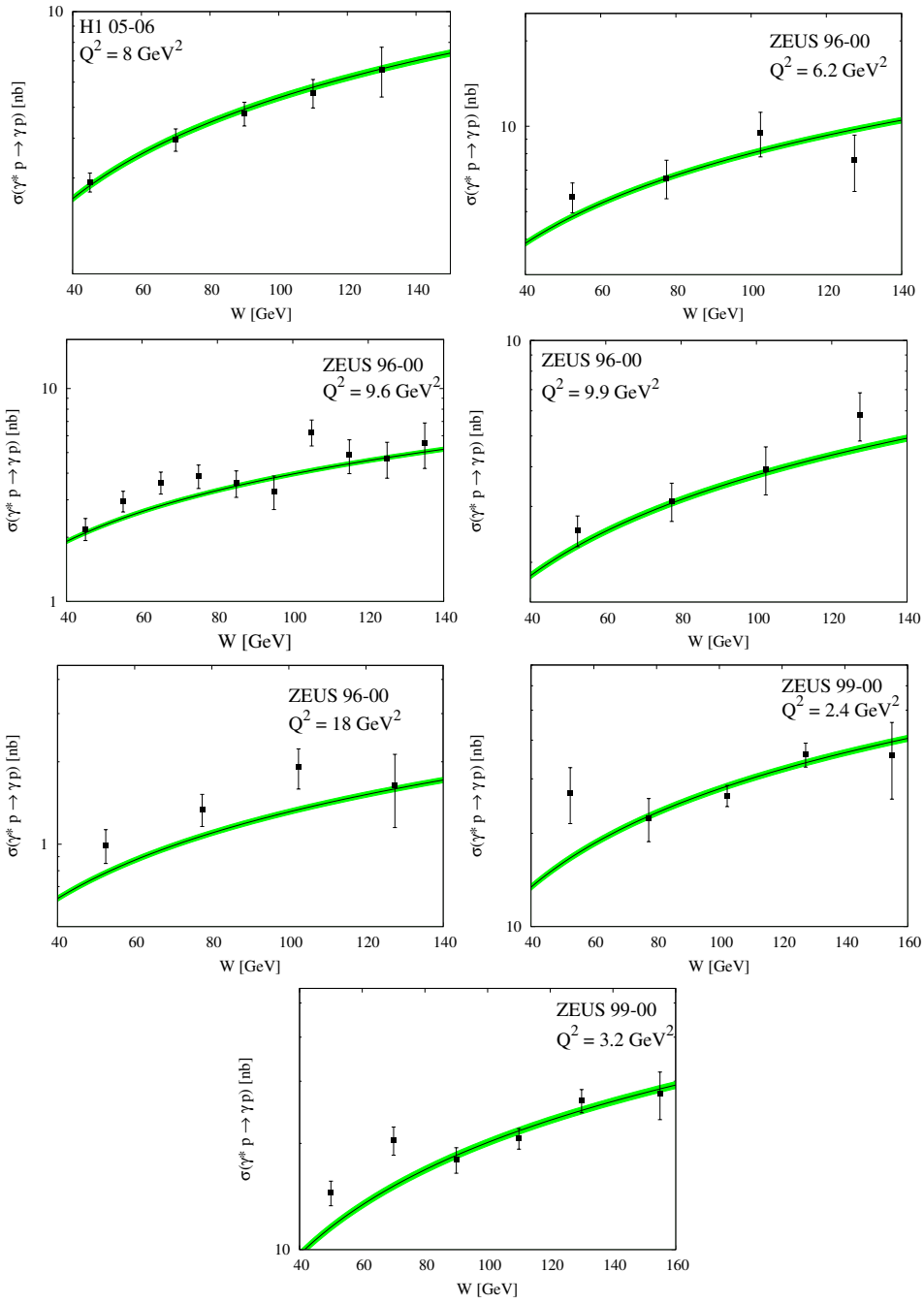

Fig. 7. Fit of Eq. (11) to the H1 and ZEUS data on the integrated cross sections for $\gamma^* p \to \gamma p$.

3.3. J/ψ meson electroproduction

Here we show a fit of the model to the HERA data on J/ψ electroproduction [11, 12]. The resulting fit is shown in Figs. 8–11, with the values of the fitted parameters and the relevant χ^2/dof, given in Table II.

TABLE II

Fitted parameters for J/ψ electroproduction.

A_0	Q_0^2	n	α_0
29.8 ± 2.8	2.1 ± 0.4	1.37 ± 0.14	1.20 ± 0.02
α'	a	b	χ^2/dof
0.17 ± 0.05	1.01 ± 0.11	0.44 ± 0.08	1.12

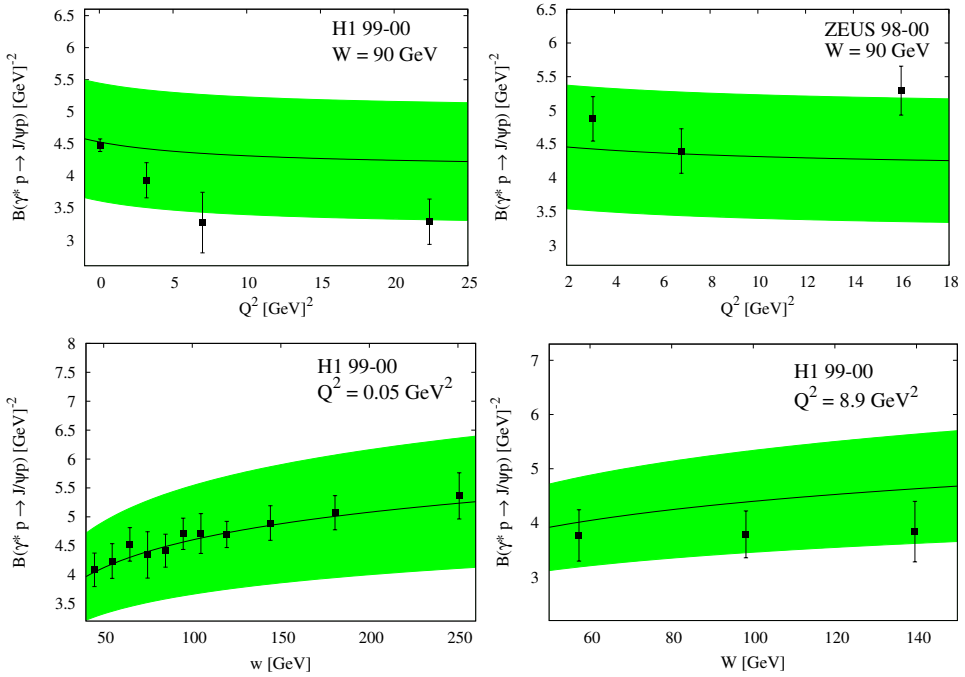

Fig. 8. Fit of Eq. (9) to the H1 and ZEUS data on the forward slopes for $\gamma^* p \to J/\psi p$.

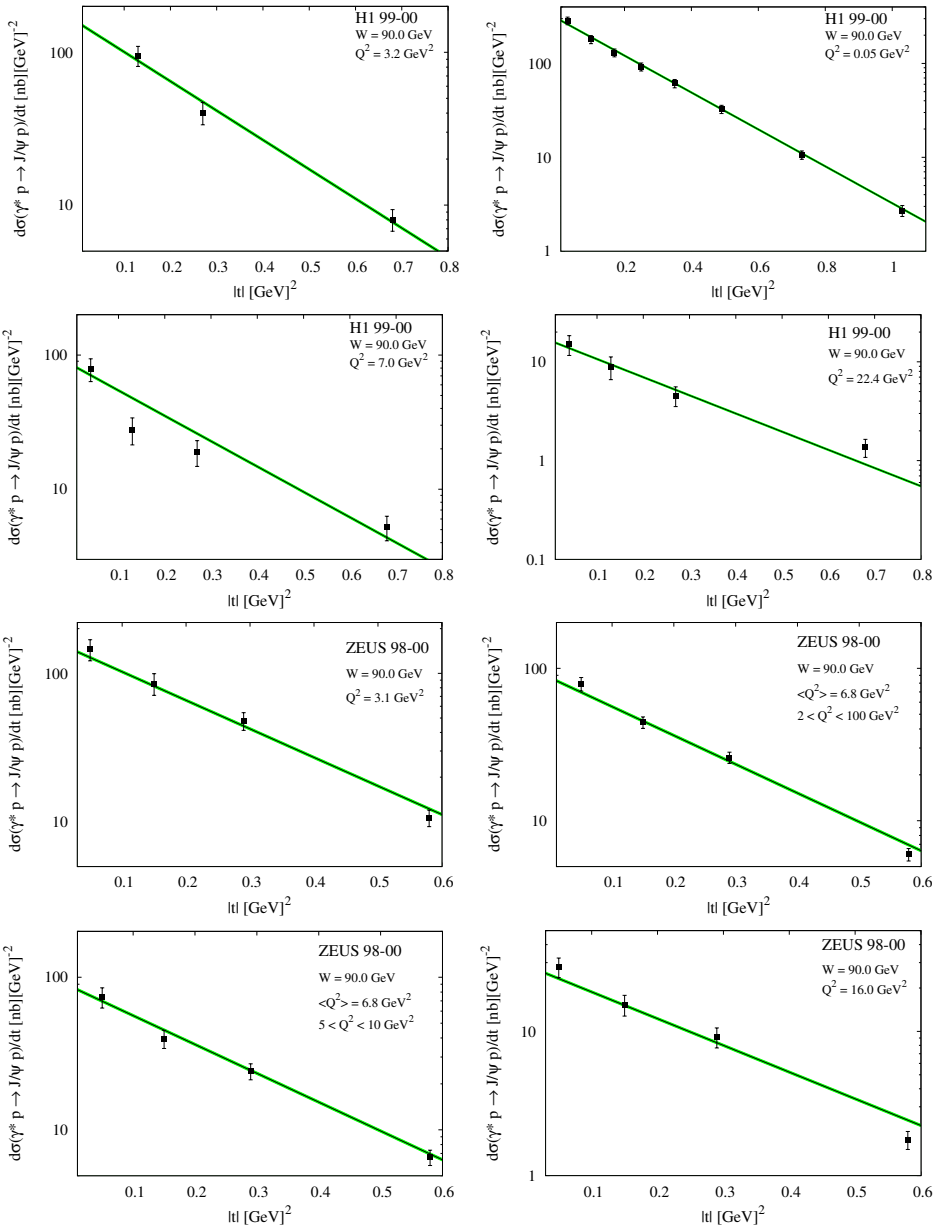

Fig. 9. Fit of Eq. (7) to the H1 and ZEUS data on the differential cross sections for $\gamma^* p \to J/\psi p$.

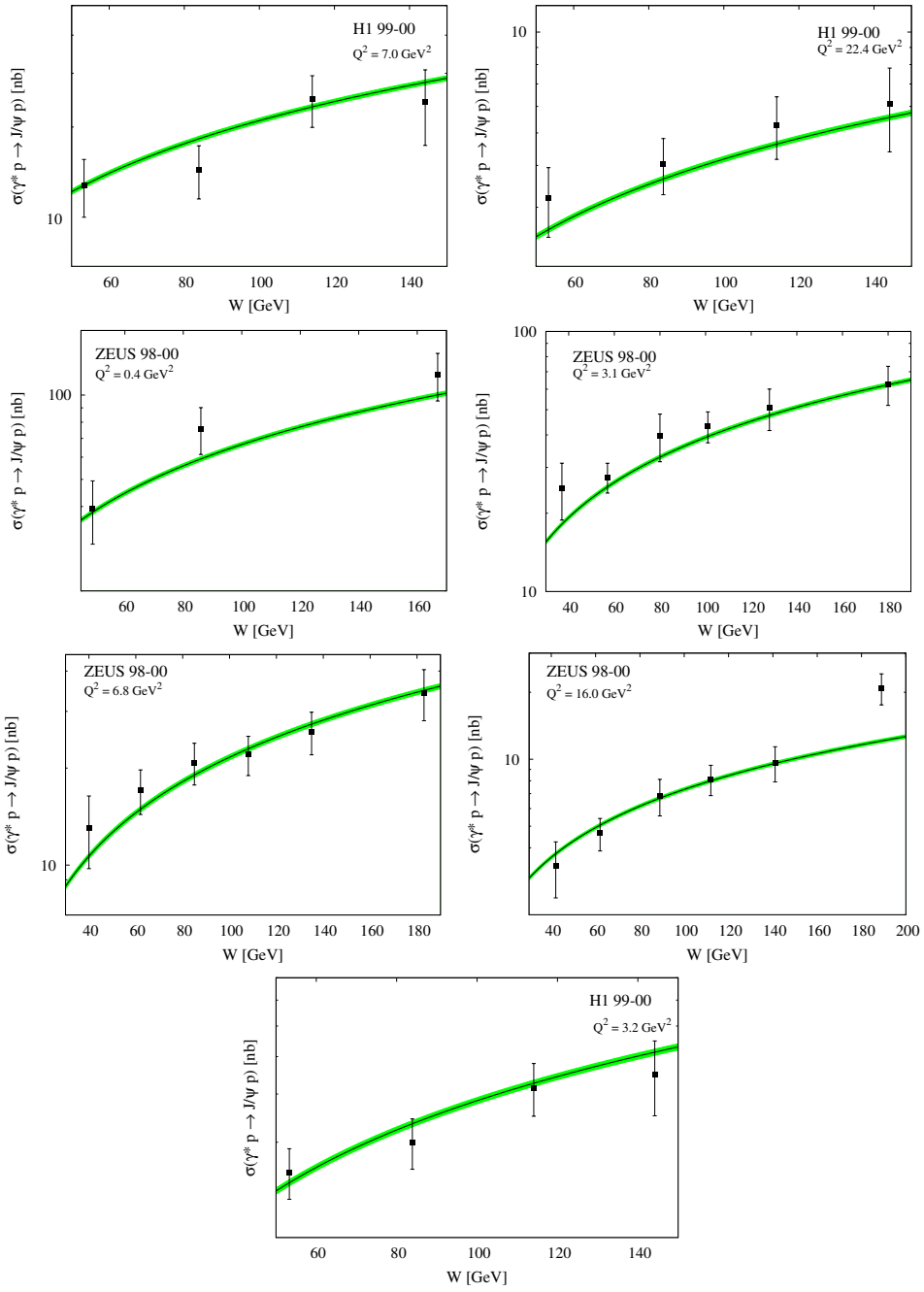

Fig. 10. Fit of Eq. (11) to the H1 and ZEUS data on the integrated cross sections for $\gamma^* p \to J/\psi p$.

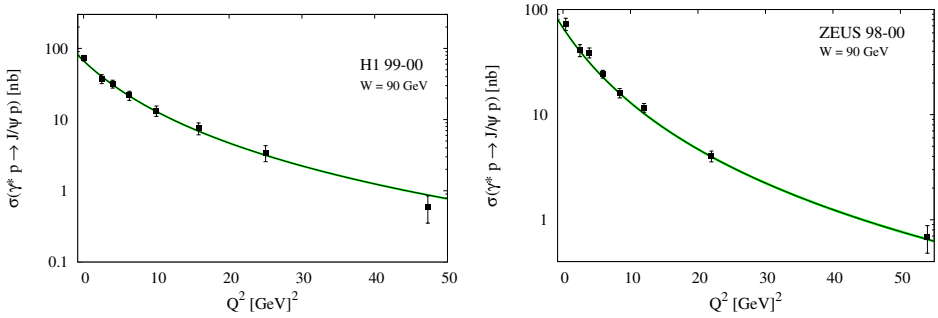

Fig. 11. Fit of Eq. (11) to the H1 and ZEUS data on the integrated cross sections for $\gamma^* p \to J/\psi p$.

3.4. ϕ meson electroproduction

Here we present a fit of the model to the HERA data on ϕ electroproduction, see [13, 14]. The resulting fit is shown in Figs. 12–14, with the values of the fitted parameters and the relevant χ^2/dof, given in Table III.

TABLE III

Fitted parameters for ϕ electroproduction.

A_0	Q_0^2	n	α_0
37.2 ± 0.7	1.7 ± 0.2	1.48 ± 0.13	1.15 ± 0.27
α'	a	b	χ^2/dof
0.10 ± 0.05	−0.09 ± 0.18	2.18 ± 0.34	0.05

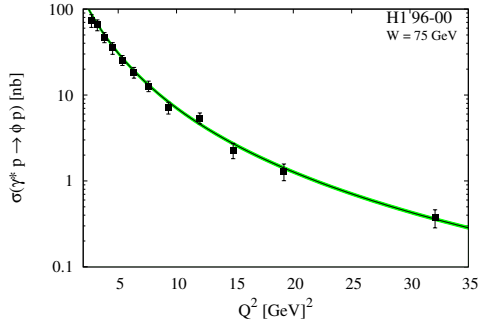

Fig. 12. Fit of Eq. (11) to the H1 data on the integrated cross sections for $\gamma^* p \to \phi p$.

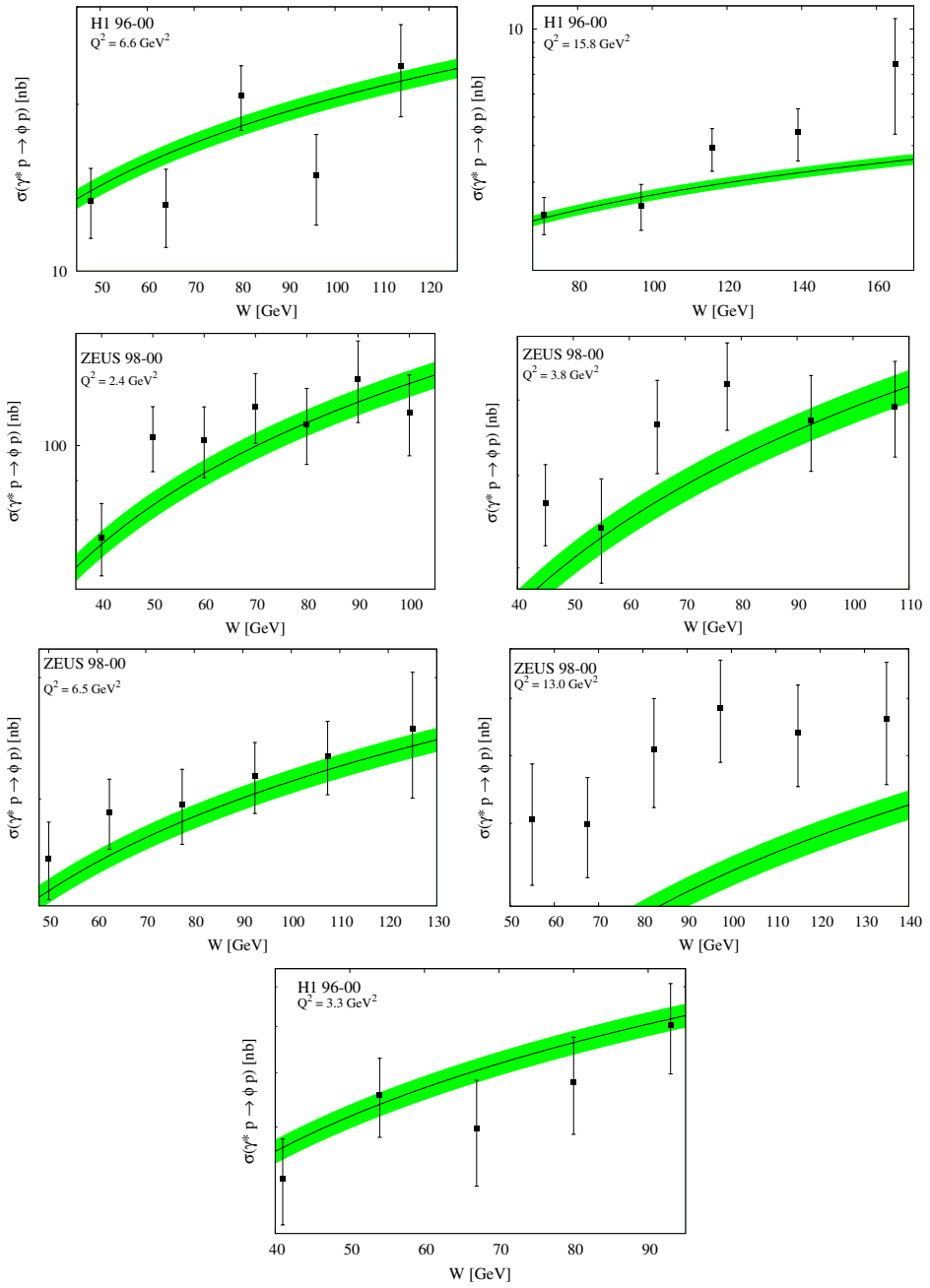

Fig. 13. Fit of Eq. (11) to the H1 and ZEUS data on the integrated cross sections for $\gamma^* p \to \phi p$.

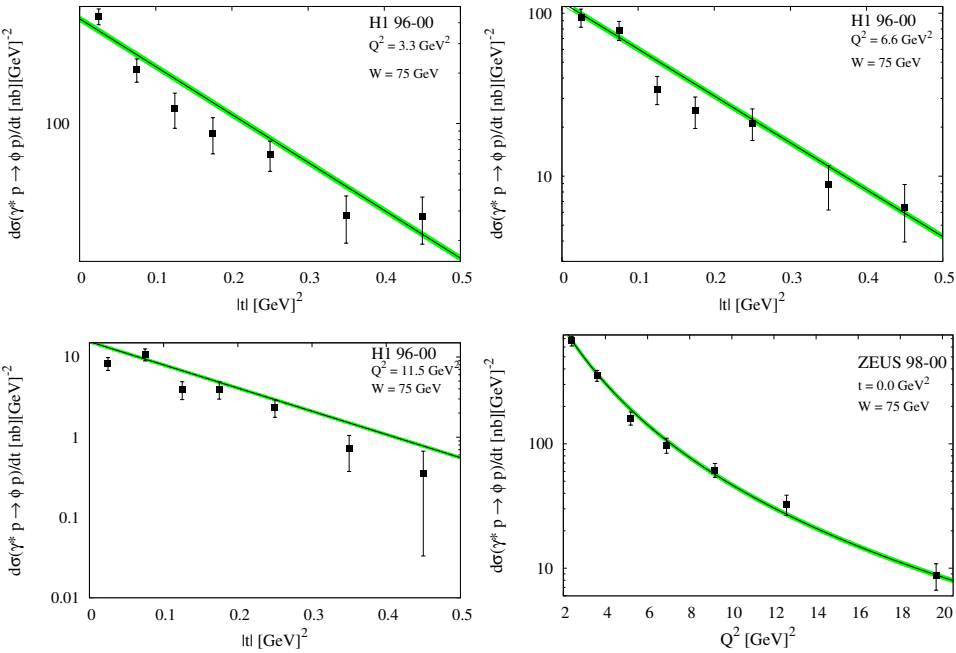

Fig. 14. Fit of Eq. (7) to the H1 and ZEUS data on the differential cross sections for $\gamma^* p \to \phi p$.

4. Conclusions and discussion

Our study shows that DVCS and each VM electroproduction reactions can be separately fitted within the present model with a single Pomeron trajectory.

Some problems arise for ϕ production at high virtualities $Q^2 \gtrsim 13$ GeV^2 (see Fig. 13). Also there are problems with fitting photoproduction and electroproduction data simultaneously for ρ (and also ϕ) production. Light mesons seem to be sensitive to the transition from the soft to the hard regime. So, these may serve as hints that it is not enough to use the current model with one-component Pomeron to describe the whole spectrum of VMP and DVCS data together. For this reason, we may need a model with two components Pomeron (*i.e.* the amplitudes with soft and hard terms), see Appendix A.

The present fits can serve as a basis (input parameters) for a global fit of the model with both soft and hard terms (see Appendix A) with a unique set of parameters for all reactions. Such work is in progress [7].

Among open problems, we mention the need for theoretical arguments to define and constrain the form of the $\widetilde{Q}^2$-dependent factor in amplitude Eq. (3) (or the H factors in front of the soft and hard terms, Eqs. (A.1), (A.3), (A.2) and (A.4) in Appendix A). These constraints may come from the QCD evolution and/or from the unitarity condition.

L.J. thanks the Department of Physics of the University of Calabria and the Istituto Nazionale di Fisica Nucleare — Gruppo Collegato di Cosenza, where part of this work was done, for their hospitality and support. He was supported also by the Project "Matter Under Extreme Conditions" of the Ukrainian National Academy of Sciences.

Appendix A

A two-component Pomeron

Following Refs. [15, 16], we comprise soft and hard dynamics within a single Pomeron which, however, has two components — a soft and a hard one, with relative $\widetilde{Q}^2$-dependent weights. These weights are constructed such as to provide the right balance between the soft and hard components, *i.e.* as $\widetilde{Q}^2$ increases, the weight of the hard term increases, and *vice versa*. These weights do not affect the Reggeometric form of the model.

The relevant scattering amplitude is

$$A\left(s,t,Q^2,{M_v}^2\right) = \frac{\widetilde{A_{\rm s}}}{\left(1+\frac{\widetilde{Q^2}}{Q_{\rm s}^2}\right)^{n_{\rm s}}} e^{-i\frac{\pi}{2}\alpha_{\rm s}(t)} \left(\frac{s}{s_{0{\rm s}}}\right)^{\alpha_{\rm s}(t)} e^{2\left(\frac{a_{\rm s}}{\widetilde{Q^2}}+\frac{b_{\rm s}}{2m_N^2}\right)t}$$
$$+ \frac{\widetilde{A_{\rm h}}\left(\frac{\widetilde{Q^2}}{Q_{\rm h}^2}\right)}{\left(1+\frac{\widetilde{Q^2}}{Q_{\rm h}^2}\right)^{n_{\rm h}+1}} e^{-i\frac{\pi}{2}\alpha_{\rm h}(t)} \left(\frac{s}{s_{0{\rm h}}}\right)^{\alpha_{\rm h}(t)} e^{2\left(\frac{a_{\rm h}}{\widetilde{Q^2}}+\frac{b_{\rm h}}{2m_N^2}\right)t}. \qquad \text{(A.1)}$$

Here, $\widetilde{A_{\rm s}}$ and $\widetilde{A_{\rm h}}$ are normalization factors, $Q_{\rm s}^2$ and $Q_{\rm h}^2$ are soft and hard scales for virtuality, $n_{\rm s}$ and $n_{\rm h}$ are free parameters to be fitted, as well as four parameters $a_{\rm s}$, $b_{\rm s}$, $a_{\rm h}$ and $b_{\rm h}$, $s_{0{\rm s}}$ and $s_{0{\rm h}}$ are soft and hard scales for the squared energy, $\alpha_{\rm s}(t)$ and $\alpha_{\rm h}(t)$ are Regge trajectories for the soft and hard components of the Pomeron.

Substituting the amplitude (A.1) into Eqs. (6) and (10), we obtain the differential and integrated cross sections which are, respectively,

$$\frac{d\sigma}{d|t|} = H_{\rm s}^2 e^{2\{L_{\rm s}(\alpha_{\rm s}(t)-1)+\mathfrak{g}_{\mathfrak{s}}t\}} + H_{\rm h}^2 e^{2\{L_{\rm h}(\alpha_{\rm h}(t)-1)+\mathfrak{g}_{\mathfrak{h}}t\}}$$
$$+2H_{\rm s}H_{\rm h}e^{\{L_{\rm s}(\alpha_{\rm s}(t)-1)+L_{\rm h}(\alpha_{\rm h}(t)-1)+(\mathfrak{g}_{\mathfrak{s}}+\mathfrak{g}_{\mathfrak{h}})t\}}\cos\left(\frac{\pi}{2}\left(\alpha_{\rm s}(t)-\alpha_{\rm h}(t)\right)\right), \qquad \text{(A.2)}$$

and

$$\sigma = \frac{H_{\rm s}^2 e^{2\{L_{\rm s}(\alpha_{0\rm s}-1)\}}}{2(\alpha'_{\rm s}L_{\rm s}+\mathfrak{g}_{\mathfrak{s}})} + \frac{H_{\rm h}^2 e^{2\{L_{\rm h}(\alpha_{0\rm h}-1)\}}}{2(\alpha'_{\rm h}L_{\rm h}+\mathfrak{g}_{\mathfrak{h}})} + 2H_{\rm s}H_{\rm h}e^{L_{\rm s}(\alpha_{0\rm s}-1)+L_{\rm h}(\alpha_{0\rm h}-1)}\frac{\mathfrak{B}\cos\phi_0+\mathfrak{L}\sin\phi_0}{\mathfrak{B}^2+\mathfrak{L}^2}\,, \tag{A.3}$$

with the notation

$$H_{\rm s} = \frac{A_{\rm s}}{\left(1+\frac{\widetilde{Q^2}}{Q_{\rm s}^2}\right)^{n_{\rm s}}}\,, \qquad H_{\rm h} = \frac{A_{\rm h}\left(\frac{\widetilde{Q^2}}{Q_{\rm h}^2}\right)}{\left(1+\frac{\widetilde{Q^2}}{Q_{\rm h}^2}\right)^{n_{\rm h}+1}}, \tag{A.4}$$

where we use $A_{\rm s,h} = \frac{\sqrt{\pi}}{s_0}\widetilde{A}_{\rm s,h}$

$$L_{\rm s} = \ln\left(\frac{s}{s_{0\rm s}}\right), \qquad \mathfrak{g}_{\mathfrak{s}} = 2\left(\frac{a_{\rm s}}{\widetilde{Q^2}}+\frac{b_{\rm s}}{2m_p^2}\right), \qquad \alpha_{\rm s}(t) = \alpha_{0\rm s}+\alpha'_{\rm s}t\,,$$
$$\mathfrak{L}_{\rm h} = \ln\left(\frac{s}{s_{0\rm h}}\right), \qquad \mathfrak{g}_{\mathfrak{h}} = 2\left(\frac{a_{\rm h}}{\widetilde{Q^2}}+\frac{b_{\rm h}}{2m_p^2}\right), \qquad \alpha_{\rm h}(t) = \alpha_{0\rm h}+\alpha'_{\rm h}t\,,$$

$$\mathfrak{B} = L_{\rm s}\alpha'_{\rm s}+L_{\rm h}\alpha'_{\rm h}+(\mathfrak{g}_{\mathfrak{s}}+\mathfrak{g}_{\mathfrak{h}})\,, \qquad \mathfrak{L} = \frac{\pi}{2}(\alpha'_{\rm s}-\alpha'_{\rm h})\,,$$
$$\phi_0 = \frac{\pi}{2}(\alpha_{0\rm s}-\alpha_{0\rm h})\,.$$

The parameters of the linear Pomeron trajectories are fixed according to Refs. [15, 16]

$$\alpha_{\rm s}(t) = 1.08+0.25t\,, \qquad \alpha_{\rm h}(t) = 1.44+0.01t\,.$$

Appendix B

A model with Q^2-dependent Pomeron trajectory

An effective way to account for the "hardening" of dynamics in the one-component model analyzed in this article is an introduction of $\widetilde{Q}^2$-dependent parameters of the Pomeron trajectory. Below, we present an example of such a treatment. Although it is not a "solution" of the problem, it may provide hints for the expected trends in the $\widetilde{Q}^2$-dependence of the amplitude.

Limiting ourselves to the DVCS case, consider the amplitude presented in Eq. (5)

$$A\left(Q^2, W, t, M_V^2\right) = \frac{A_0}{\left(1+\widetilde{Q}^2/Q_0^2\right)^n} e^{-\frac{i\pi}{2}\alpha(t)} (s/s_0)^{\alpha(t)} e^{-2\left(\frac{a}{\widetilde{Q}^2}+\frac{b}{2m_p^2}\right)|t|}. \tag{B.1}$$

Here, we fix $Q_0^2 = 1.0$ GeV^2 and $s_0 = 1.0$ GeV^2, so that A_0, n, a and b remain the only free parameters.

We use a linear Pomeron trajectory, $\alpha(t, Q^2) = \alpha_0(\widetilde{Q}^2) + \alpha'(\widetilde{Q}^2)t$, where the $\widetilde{Q}^2$-dependence of its parameters mimics the "hardening" of the reactions.

We define the intercept of the Pomeron trajectory as

$$\alpha_0\left(\widetilde{Q}^2\right) = \frac{1}{\ln\left(d + \frac{1}{f+\widetilde{Q}^2}\right)}, \tag{B.2}$$

with $d = 2.16$ and $f = 2.744$ providing for the "soft" cross section limit

$$\alpha_0\left(\widetilde{Q}^2 = 0\right)\Big|_{\text{DVCS}} = \frac{1}{\ln\left(2.16 + \frac{1}{2.744}\right)} = 1.08,$$

and the "hard" cross section limit

$$\alpha_0\left(\widetilde{Q}^2 \to \infty\right)\Big|_{\text{DVCS}} = \frac{1}{\ln(2.16)} = 1.3.$$

Similarly, we introduce the "soft" and "hard" limits in the slope of the Pomeron trajectory as

$$\alpha'\left(\widetilde{Q}^2\right) = \ln\left(1 + \frac{1}{\left(c+\widetilde{Q}^2\right)}\right), \tag{B.3}$$

with $c = 8.17$, such that

$$\alpha'\left(\widetilde{Q}^2 = 0\right)\Big|_{\text{DVCS}} = \ln\left(1 + \frac{1}{8.17}\right) = 1.12,$$

and

$$\alpha\left(\widetilde{Q}^2 \to \infty\right)\Big|_{\text{DVCS}} = \ln(1) = 0.$$

Using the above formulas for the cross sections and the forward slope (see Eqs. (11), (7) and (9)), with the $\widetilde{Q}^2$-dependent parameters of Pomeron trajectory, we have fitted this model to the HERA data.

From the fitting of the DVCS forward slope, we obtained: $a = 0.27$, $b = 1.98$, $\chi^2/\text{dof} = 0.11$. At this point, all parameters: a, b, c, d, f are fixed except for the normalization A_0 and the exponent n.

Fitting this model to the DVCS elastic cross section, we find: $A_0 = 16.2$, $n = 1.43$ (see also [5, 6]).

REFERENCES

[1] I.P. Ivanov, N.N. Nikolaev, A.A. Savin, *Phys. Part. Nucl.* **37**, 1 (2006) [arXiv:hep-ph/0501034].

[2] R. Fiore, L.L. Jenkovszky, F. Paccanoni, *Eur. Phys. J.* **C10**, 461 (1999) [arXiv:hep-ph/9812458].

[3] M. Capua *et al.*, *Phys. Lett.* **B645**, 161 (2007) [arXiv:hep-ph/0605319].

[4] S. Fazio, R. Fiore, L.L. Jenkovszky, A. Lavorini, *Phys. Rev.* **D85**, 054009 (2012) [arXiv:hep-ph/1109.6374].

[5] S. Fazio *et al.*, *Reggeometry of Deeply Virtual Compton Scattering and Exclusive Diffractive Vector Meson Production at HERA*, in: Recontres du Viet Nam, 14-th Workshop on Elastic and Diffractive Scattering, Eds. M.A. Rotondo, Ch.-I. Tan, SLAC eConf C111215.

[6] R. Fiore, L.L. Jenkovszky, A. Lavorini, A. Salii, in the Proceedings of "Diffraction 2012: International Workshop on Diffraction in High Energy and Nuclear Physics", Puerto del Carmen, Spain, September 10–15, 2012.

[7] S. Fazio *et al.*, work in progress.

[8] A. Atkas *et al.* [H1 Collaboration], *Eur. Phys. J.* **C44**, 1 (2005) [arXiv:hep-ex/0505061].

[9] F.D. Aaron *et al.* [H1 Collaboration], *Phys. Lett.* **B681**, 391 (2009) [arXiv:0907.5289 [hep-ex]].

[10] S. Chekanov *et al.* [ZEUS Collaboration], *J. High Energy Phys.* **0905**, 108 (2009) [arXiv:0812.2517 [hep-ex]].

[11] S. Chekanov *et al.* [ZEUS Collaboration], *Nucl. Phys.* **B695**, 3 (2004) [arXiv:hep-ex/0404008].

[12] A. Atkas *et al.* [H1 Collaboration], *Eur. Phys. J.* **C46**, 585 (2006) [arXiv:hep-ex/0510016].

[13] F.D. Aaron *et al.* [H1 Collaboration], *J. High Energy Phys.* **1005**, 032 (2010) [arXiv:0910.5831 [hep-ex]].

[14] S. Chekanov *et al.* [ZEUS Collaboration], *Nucl. Phys.* **B718**, 3 (2005) [arXiv:hep-ex/0504010].

[15] P.V. Landshoff, *Acta Phys. Pol. B* **40**, 1967 (2009) [arXiv:0903.1523 [hep-ph]].

[16] A. Donnachie, P.V. Landshoff, arXiv:0803.0686 [hep-ph].